We are IntechOpen, the world's leading publisher of Open Access books Built by scientists, for scientists

4,800
Open access books available

122,000
International authors and editors

135M
Downloads

Our authors are among the

154
Countries delivered to

TOP 1%
most cited scientists

12.2%
Contributors from top 500 universities

CLARIVATE ANALYTICS BOOK CITATION INDEX INDEXED

WEB OF SCIENCE™

Selection of our books indexed in the Book Citation Index in Web of Science™ Core Collection (BKCI)

Interested in publishing with us?
Contact book.department@intechopen.com

Numbers displayed above are based on latest data collected.
For more information visit www.intechopen.com

Chapter 11

Application of Mass Transfer Models in Environmental Engineering

Pen-Chi Chiang and Shu-Yuan Pan

Additional information is available at the end of the chapter

http://dx.doi.org/10.5772/60917

Abstract

Generally, unit operation processes that are used in environmental engineering are involved in interfacial reaction where mass transfer is an extremely essential component for system optimization. The purposes of this chapter were intended to provide the information of both theoretical model development and engineering practice for mass transfer of important processes in environmental engineering. Those processes include, but are not limited to, (1) ozonation (gas–liquid process), (2) ion exchange (liquid–solid process), (3) biological activated carbon (liquid–solid process), (4) chlorination (gas–liquid process), and (5) carbonation (gas–liquid–solid process).

Keywords: ozonation, ion exchanger, biological activated carbon, chlorination, carbonaion, rotating packed bed

1. Introduction

1.1. Ozonation process

1.1.1. Model development

1.1.1.1. Process chemistry

Ozone process has been utilized in thousands of water treatment applications such as municipal water (or wastewater) treatment plants, cooling towers, ultrapure water, marine aquaria, beverage industries, industrial process water, swimming pools, bottled-water plants, aquaculture, and food processing. It can oxidize the micro-pollutants and reduce the amount of disinfection by-product (DBP) precursors formed in drinking water [1], such as organic peroxides, aliphatic aldehydes, hydrogen peroxides, mixed functional and saturated carbox-

ylic acids, etc. Some of the DBPs such as aldehydes and/or chlorinated aldehydes would be potential health hazards, leading to the increase of bacterial populations in distribution systems. Three oxygen molecules will combine together to form ozone, as shown in Equation (1); this is an endothermic reaction:

$$2O_3 \leftrightarrow 3O_2,\ \Delta H^0 = +284.5\ \text{kJ/mol}\ (\text{at 1 atm}) \tag{1}$$

The gaseous ozone (O_3) will decompose to oxygen gas (O_2), as shown in Equation (2). In general, the decomposition rate increases as the temperature increases. The efficiency of ozone production decreases at a higher temperature with a fixed voltage input.

$$O_3 + O_2 \rightarrow O_2 + O_2 + O \tag{2}$$

1.1.2. Reaction kinetics and mass transfer

Ozonation is a gas–liquid process under dynamic conditions; the reaction regime, mass transfer characteristics, and reaction kinetics are critical to system design and operation. As O_3 dissolves in water, it will self-decompose and generate oxygen and hydroxyl-free radicals. In general, the solubility of dissolved O_3 in ozonated water is merely 1 mg/L; higher dissolved O_3 concentration will only happen in the environment with better mass transfer (e.g., mixing). The mass transfer rate is influenced by operating variables such as pH, temperature, agitation speed, and gas flow rate. In general, the ozone concentration generated from ozone generator usually is less than 14 % (v/v) that may restrict the mass transfer between gas and liquid phases. Therefore, residual ozone concentration in water treatment ranges from 0.1 to 1 mg/L. A higher dissolved ozone concentration may happen only if under better mass transfer conditions.

It is noted that the specific interfacial area is of great significance to the gas–liquid mass transfer. In ozonation process, the overall liquid-phase mass transfer coefficient (K_La) and equilibrium dissolved ozone concentration ($[O_3]^*$) can be obtained from the following mass balance equation [2]:

$$\frac{d[O_3]}{dt} + r_{O_3,sd} = K_L a([O_3]^* - [O_3]) \tag{3}$$

where $r_{O3,sd}$ is the self-decomposition rate of ozone, which can be determined by Yang [3] as Equation (4):

$$\begin{aligned} r_{O_3,sd} &= 5.117 \times 10^{10} \exp\left(-\frac{8835.25}{T}\right)[O_3] + 9.207 \\ &\times 10^{16} \exp\left(-\frac{8835.25}{T}\right)[OH^-]^{0.5}[O_3] \end{aligned} \tag{4}$$

http://dx.doi.org/10.5772/60917

where *T* is the temperature (K). With the known $[O_3]$, t, and $r_{O3,sd}$, both the K_La and $[O_3]^*$ can be determined through the use of a linear regression analysis under specific experimental conditions.

1.2. Engineering practice

1.2.1. Determination of overall mass transfer coefficients

Figure 1 presents a typical schematic diagram of ozonation process, where the ozone is produced by an ozone generator and able to reach 10 % or higher.

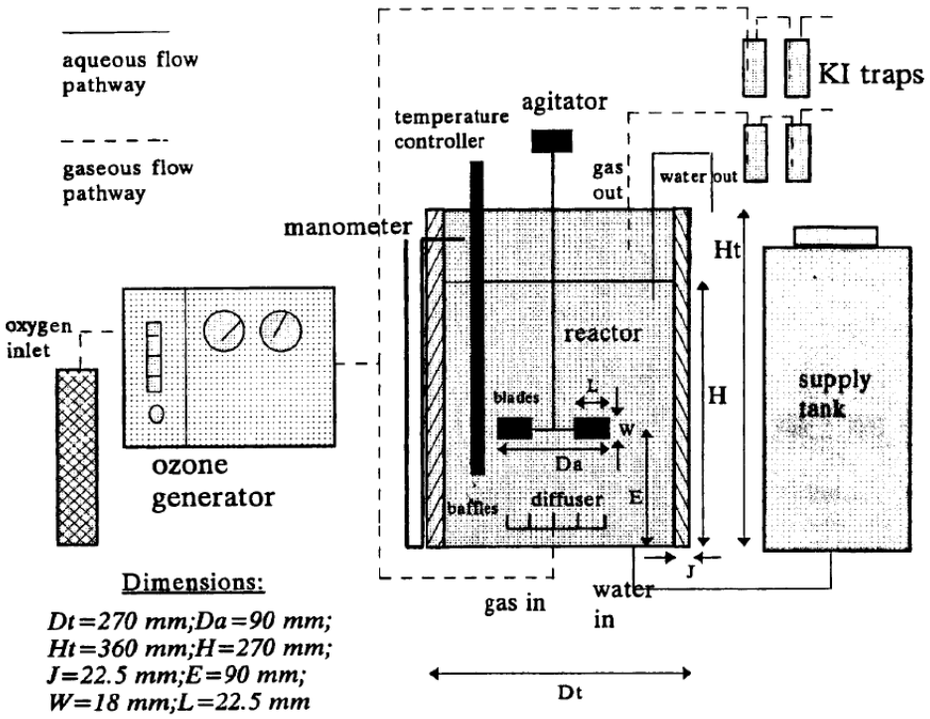

Figure 1. Schematic diagram of ozone experimental system (adapted from Chiang et al. [2])

Ouederni et al. [4] proposed the following equation to determine the ozone transfer in stirred reactors:

$$K_L a = 2.57 \times 10^{-2} \times (nG)^{0.67} \tag{5}$$

where K_La is expressed in s^{-1}, G is the gas flow rate expressed in 10^{-3} m^3/s, and n is the number of rotations per second. According to Sheffer and Esterson [5], the volumetric overall liquid-phase mass transfer coefficient of ozone in tap water (K_La) was around 1.14 min^{-1}. It was also observed that it would reach a higher value at a higher water flow rate (i.e., sufficient agitation). For instance, there was a large decrease in K_La to 0.25 min^{-1} without agitation.

In addition, combining the empirical relationship reported by Stankovic [6], the following equation can be derived:

$$K_L a = h \cdot D_v^{0.5} \cdot n^{0.5} \cdot G^x \tag{6}$$

where h and x are constants, a is the specific interfacial area (cm^{-1}), and G is the influent gas flow rate (L min^{-1}).

1.2.2. Determination of Fractional Ozone Absorption (FOA)

To determine the optimal operation conditions for semi-batch ozonation process, the "fractional ozone absorption (FOA)," defined as the ratio of the ozone transferred to water to the ozone applied to the reactor [7], should be applied. The FOA value in semi-batch operation can be expressed as [2]

$$FOA(\%) = \frac{V \times K_L a \times ([O_3]^* - [O_3])}{G \times P_{O_3} \times 1.98 \times 10^5} \times 10 \tag{7}$$

where P_{O3} is the ozone partial pressure (kPa). The value of 1.98 x 10^5 is the factor which will transfer the term of denominator into the unit of mg/min.

An increase in temperature will increase the ozone diffusivity in water and enhance the liquid-phase mass transfer, because the K_L value is directly proportional to $Dv^{0.5}$ based on Higbie's penetration theory [8].

Figure 2 shows the relationships between the agitation speeds and influent gas flow rates under the specific conditions of $K_L a$ and FOA_0. The results indicate that the FOA_0 is mainly controlled by n (not by G). Both the values of $K_L a$ and FOA_0 (i.e., initial *FOA*) increase as the agitation speeds increase due to the breakdown of liquid film resistance and the enhancement of surface renewal rates. Therefore, the $K_L a$ increased with the increase of the influent gas flow rate since the specific interfacial surface area between gas and liquid phases increases. In addition, Figure 2 provides the baseline information of engineering to obtain the best achievable alternative among the various scenarios of n, G, and $K_L a$ values, in terms of the same level of FOA_0. Furthermore, the desired FOA_0 in the water treatment plants can be determined by the agitation speed, if the value of G is given.

The power consumption (P_g) should be taken into consideration for the most efficient design and operating conditions in practice. P_g can be calculated as follows [9]:

$$P_g = \alpha \times N_p \times n^3 \times d_i^5 \times \rho \tag{8}$$

where P_g is the power consumption with gas dispersion (watt) and α is the ratio of P_g over P_0, where P_0 is the power consumption in un-gassed liquid. Moreover, α is a function of superficial gas velocity so it is directly proportional to G.

http://dx.doi.org/10.5772/60917

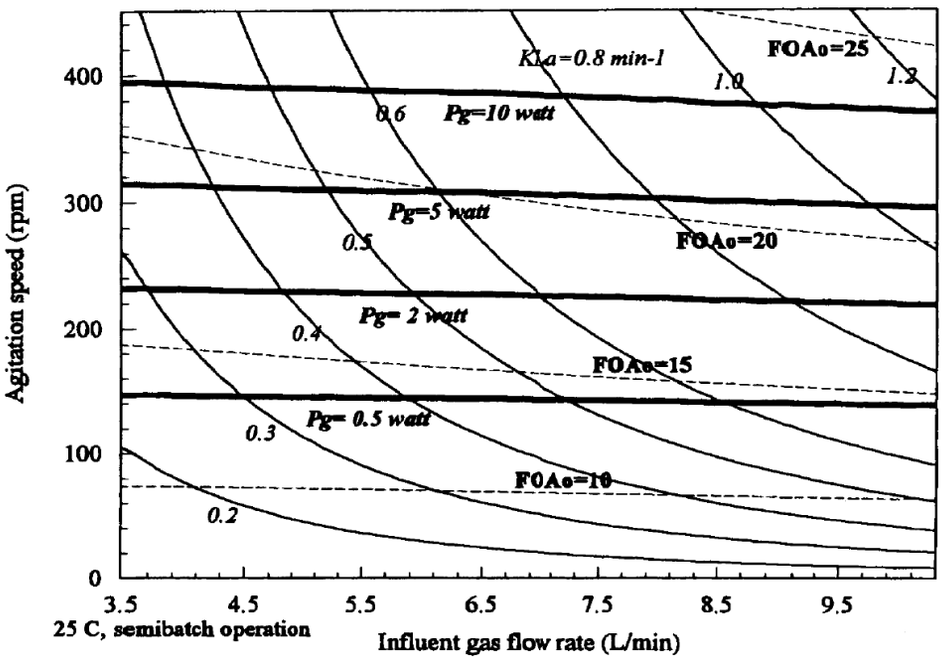

Figure 2. Effect of agitation speeds and influent gas flow rates on K_La, initial fractional ozone absorption (FOA_0), and power consumption. (Adapted from Chiang et al. [2])

N_p is the power number:

$$N_p = \frac{P_0}{n^3 \times d_i^5 \times \rho} \tag{9}$$

Figure 2 can be used to determine *G* and *n* for given requirements of FOA_0 and P_g, since the P_g value is influenced by both *n* and *G*. Under a constant value of *G*, the optimum operation conditions for semi-batch operation can be determined. For a standard six-bladed turbine with an N_p value of 5.2 [9], the desired value of α can be determined corresponding to various G values.

1.2.3. Integration of mass transfer and reaction kinetics

Two important factors for determining the kinetic regime of ozonation are the enhancement factor (*E*) and Hatta number (*Ha*). The *E* factor is defined as the ratio between the apparent reaction and the maximum physical absorption rates:

$$E = \frac{N_t}{K_L a[O_3]^*} \tag{10}$$

where *Nt* is the actual ozone absorption rate (M s^{-1}) and K_La is the overall mass transfer coefficient (s^{-1}). The $[O_3]^*$ values can be determined from Henry's constant and the ozone partial pressure at the reactor outlet. On the other hand, the Ha number for O_3 reaction is defined as

$$Ha = \sqrt{\frac{k_1[O_3]^* D_{O_3,L}}{k_L{}^2}} \tag{11}$$

DeCoursey [10] proposed a correlation between E and Ha for irreversible second-order reactions based on the Danckwerts penetration model, which takes the form as follows:

$$E = -\frac{Ha^2}{2(E_\infty - 1)} + \sqrt{\frac{Ha^4}{4(E_\infty - 1)^2} + \frac{E_\infty \cdot Ha^2}{(E_\infty - 1)} + 1} \tag{12}$$

where E_∞ is the infinite mass transfer enhancement factor. It is also noted that the expression is particularly accurate as the diffusivity coefficients of the reactants in the liquid are of the same order of magnitude.

Since the prediction model of K_La is applicable only to the deionized water, it is necessary to introduce the enhancement factor (E) to account for the effect of organic compounds in the real water sample on K_La. The n value (rps) for the fixed level of water quality parameters, applied ozone concentration [O_3], and influent gas flow rate (Q) can be developed as

$$n = \left(\frac{Q[O_3] + Vr_{O_3}}{1.20 \times EV\left(\frac{P_{O_3}}{0.38} - [O_3]\right)} - 0.0225 \right)^2 D_v^{-1} G^{-236} \tag{13}$$

Therefore, the marginal level of ozone partial pressure (P_{O3}) to achieve the highest removal of TOC can be determined through Equation (13). It is also noted that the mass transfer is successfully incorporated with reaction kinetics characterizations in Equation (13) for predicting the optimal n value (i.e., the most efficient agitation) to control the formation potential of organic compounds in the ozonation process.

Figure 3 gives the relationship between the agitation speed and applied ozone concentration under various retention times. For example, the TOC removal efficiency of 15 % and enhancement factor (E = 1) were held constant under the temperature of 25 °C, a pH value of 7, and an influent gas flow rate of 10 L/min. The higher the ozone partial pressure, the lower the agitation speed needed to achieve the same level of performance. In other words, it suggests that the ozone partial pressure (P_{O3}) should slightly increase, instead of greatly enhancing the agitation power consumption, to obtain the same level of removal efficiency of TOC.

http://dx.doi.org/10.5772/60917

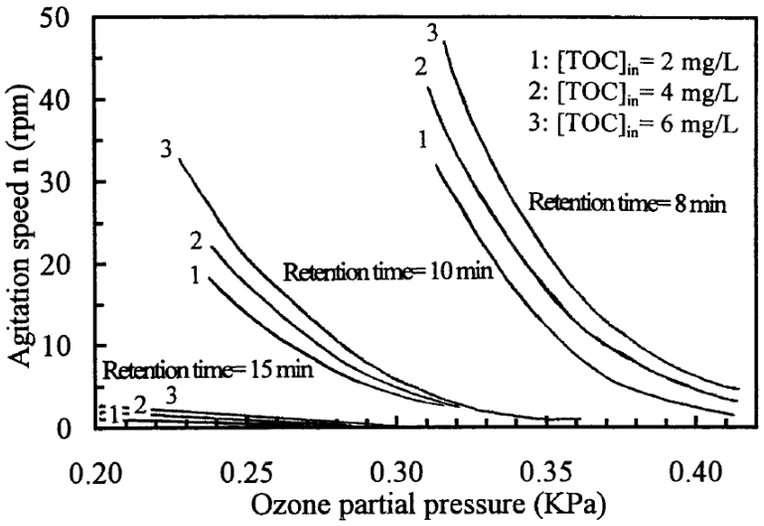

Figure 3. Simulation results of the relationship between agitation speed and ozone partial pressure in view of controlling the formation of TOC. (Chiang et al. [2])

2. Ion Exchange (IE)

Deionization is the process of removing the alts of electrolytes from water by ion exchange. "Deionization" is generally considered synonymous with "demineralization," by various authors, but since some of the ions exchanged are not necessarily of mineral origin, the term "deionization" appears more inclusive.

2.1. Model development

2.1.1. Rate-determining step

According to the Nernst static diffusion film theory, three mechanisms might be the rate-determining step under appropriate conditions:

1. Film diffusion (F-mechanism): transport of ions from the bulk liquid to the liquid solid interface
2. Particle diffusion (P-mechanism): transport of ions into the resin particle
3. Chemical reaction (C-mechanism): the chemical process of exchange

Recently, the principle of ion exchange kinetics has been investigated by applying either empirical rate equations or theoretical equations derived from fundamental diffusional mechanisms. In the latter approach, the rate-determining step could have been film diffusion, surface chemical reaction, or particle diffusion.

According to the kinetics of anion exchange on various resins, diffusion was the rate-controlling process in all cases. Turse and Rieman III [11] reported that the rate of exchange was

controlled by the chemical reaction if chelates were formed by cations and resins. Without formation of chelates, at low concentration, the rate was controlled by "film" diffusion and, on the other hand, at high concentration by "particle" diffusion. In other words, the rate-determining step of the ion exchange process is always a combination of these two limiting steps of film diffusion and particle diffusion, except for the case of large organic ions (quaternary ammonium ions) which are controlled by particle diffusion.

2.1.2. Crank model

The derivation of the Crank model is given below. For particle-diffusion controlled, the rate of exchange could be expressed as Fick's second law as follows:

$$\mathrm{D}\frac{\partial^2}{\partial r^2}(rc)=\frac{\partial}{\partial t}(rc) \tag{14}$$

With the initial condition:

$$\mathrm{C}=0, 0 \le \mathrm{r} \le \mathrm{a}, \mathrm{t} \le 0 \tag{15}$$

and the boundary condition:

$$\left(\frac{\partial r}{\partial t}\right)_{r=0}=0,\ t>0 \tag{16}$$

Equation (14) can be easily solved by the Laplace transform. The *F (t)*, fraction of the electrolyte uptake by the resin, is expressed as [12]

$$F(t)=1-\sum_{m=1}^{\infty}\frac{6\sigma(\sigma+1)}{9+9\sigma+\sigma^2 q_n{}^2}\exp\left[-\left(D_p q_n{}^2+\frac{1}{\sigma^2}\right)\right] \tag{17}$$

where $D_p{}^2$ is the diffusion coefficient. q_ns are the nonzero roots of Equation (17) as follows:

$$\tan(q_n)=\frac{3q_n}{3+\sigma q_n{}^2} \tag{18}$$

In addition, $\sigma$is the ratio of the solute in the external solution to that in the resin particles at equilibrium, which can be determined by Equation (19):

$$\sigma = \frac{3V}{4a^3K} \tag{19}$$

where K is the partition factor. Therefore, the diffusion coefficient can be determined with the aid of F (t) vs. $D_p t/a^2$, which is given by Crank (1957).

Huang and Tsai [13] have developed a more appropriate and general equation which combined film diffusion, particle diffusion, and chemical surface reaction on the exchange rate for a finite bath. Under a specified case, the rate equation (Table 1) using only isotopic exchange with particle resistance is consistent with the Crank model [12].

Models	Particle diffusion (P-mechanism)	Film diffusion (F-mechanism)	Chemical reaction (C-mechanism)
Kressman and Kitchener (Limited bath)	$\frac{Q^\tau}{Q_\infty} = \frac{6}{r}\frac{Q}{Q_0 - Q_\infty}\frac{Dpt}{\pi}$	$\frac{Q_\infty}{Q^0}\mathrm{In}\left(1-\frac{Q^\tau}{Q_\infty}\right)K_f t$	$\mathrm{In}\ Z = \frac{2KQ^0(Q^0-Q_\infty)t}{Q_\infty}$ where $Z = \frac{t(Q^0-2Q_\infty)+Q^0Q_\infty}{Q^0(Q_\infty-Q_t)}$
Yagi and Kunii (Shell progressive)	$t = \frac{Q\cdot r^2}{6Dpc}[3-3(1-X)^{2/3}-2X]$	$t = \frac{Qr}{3K_fC}X$	$t = \frac{Q}{K_sC}[1-(1-X)^{1/3}]$
Boyd (Shallow bed)	$F = 1-\frac{6}{\pi^2}\sum_{n=1}^{\infty}\frac{1}{n^2}\exp(-n^2\pi^2 t)$	$\mathrm{In}(1-F) = -3t$	$\mathrm{In}(1-F) = -t$
Crank (Finite bath)	$F = 1-\sum_{n=1}^{\infty}\frac{6\sigma(\sigma+1)\exp(-Dpq_n^2 t/a^2)}{9+9\sigma+q_n^2\sigma^2}$	$\mathrm{In}(1-F) = -3\left(1+\frac{1}{\sigma}\right)t$	$\mathrm{In}(1-F) = -\left(1+\frac{1}{\sigma}\right)t$

Table 1. Rate equation of isotopic ion exchange reaction with particle diffusion (P-mechanism), film diffusion (F-mechanism), and chemical reaction (C-mechanism) for various mathematical models

2.2. Engineering practice

2.2.1. Determination of rate-determining steps

In this chapter, the HPC and BHDAC are demonstrated as the representative quaternary ammonium ions because they are easy to prepare, highly soluble in water, and can be rapidly analyzed by use of UV. In addition, Dow-50-X8 was utilized as the resin for illustration. By plotting the θ_t/θ_∞ for HPC and BHDAC on each Dow-50-X8 resin (i.e., 20–50, 50–100, and 100–200 mesh), one can observe three straight lines with slopes of K (the parabolic rate constant). Subsequently, a liner correlation can be found between K and 1/D (the reciprocal of resin diameter), as shown in Figure 4. It suggests that the rate-determining step of these quaternary ammonium ions on the strong acid cation exchanger was particle-diffusion controlled.

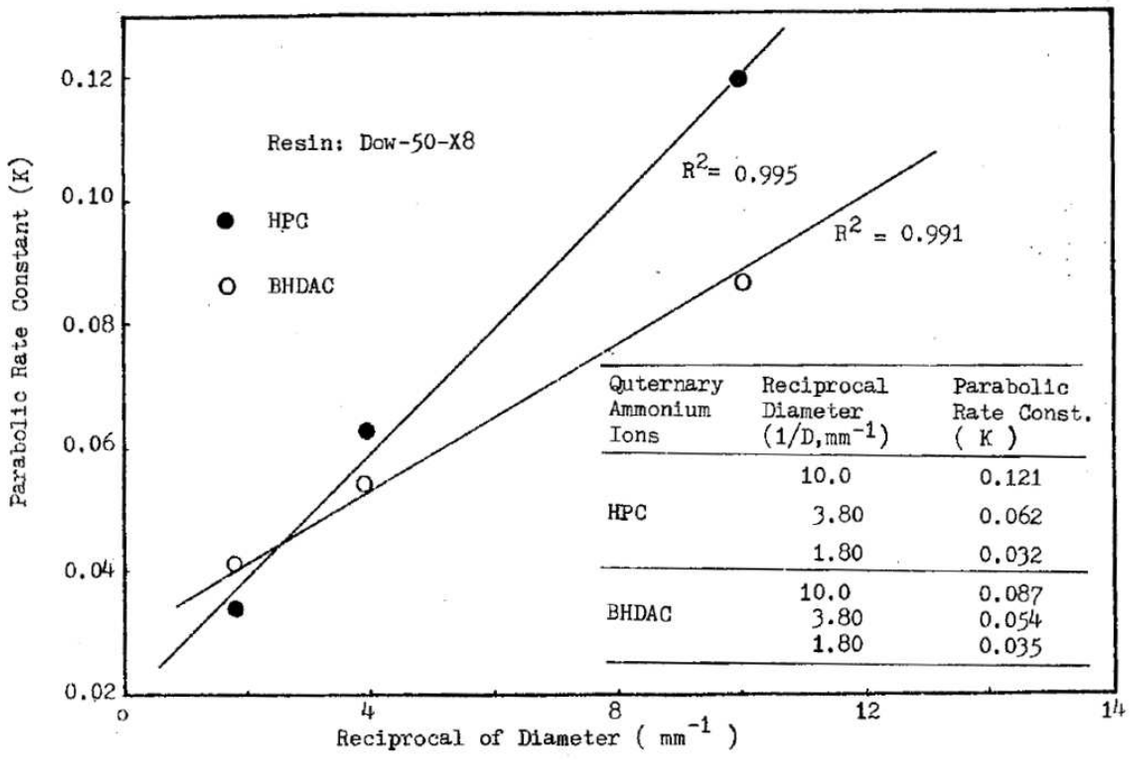

Figure 4. Effect of particle size on parabolic rate constant (resin: Dow-50-X8)

2.2.2. Determination of particle-diffusion coefficient

The particle-diffusion coefficients of LPC, HPC, and BHDAC through the Amb-200, Amb-DPI, and Dow-50-X8 resins were determined and summarized in Table 2. As previously cited, the rate of exchange of HPC and BHDAC on various particle sizes on Dow-50-x8 resins was shown in Figure 4. It was observed that the Dow-50-X8 resin possessed the lowest particle-diffusion coefficient in comparison with the Amb-200 and Amb-DPI resins. This evidence strongly suggested that the macroporous resin had an advantage over the gel-structure resins for exchange of organic ions.

Quaternary ammonium ions	**Amb-200** (10^9 cm^2/sec)	**Amb-DPI** (10^9 cm^2/sec)	**Dow-50-X8** (10^9 cm^2/sec)
LPC	3.03	2.35	-
HPC	2.43	2.12	0.85
BHDAC	0.90	1.70	0.57

Table 2. Particle-diffusion coefficient of LPC, HPC, and BHDAC through the Amb-200, Amb-DPI, and Dow-50-X8 resins (20–50 mesh)

http://dx.doi.org/10.5772/60917

It was thus concluded that the Amb-200 (strong acid cation exchanger), Amb-DPI (weak acid cation exchanger), and XE-318 (chelating cation exchanger) resins were the ones to be selected as the representative cation exchangers for the resin selectivity test as described later.

3. Biological Activated Carbon (BAC)

3.1. Model development

3.1.1. Representative models of BAC

The biological activated carbon (BAC) process contains adsorption and biodegradation mechanisms. The BAC process also exhibits lower regeneration cost and prolongs the life of granular activated carbon (GAC) beds. Therefore, it has been widely used in water and wastewater treatments.

A well-validated mathematical model can provide valuable information to evaluate and predict the performance of BAC process. Table 3 presents several representative models for BAC process. Chang and Rittmann [14] developed a model that the mass transfer of substrates diffusing through the biofilm, metabolized by microbes, and finally reaching the surface of GAC was illustrated and quantified. However, the limitation of the model is that it cannot be used under unsteady or plug flow conditions. Sakoda et al. (1996) developed a theoretical model for a BAC column considering the mechanisms including dispersion, convection, biodegradation, and adsorption. The assumption included that the substrate concentration on the interface between the biofilm and the GAC is identical to that in the bulk solution. Furthermore, Liang and Chiang [15] developed a non-steady-state numerical model to differentiate the adsorption and biodegradation quantities of a continuous BAC column including the mechanisms of adsorption, biodegradation, convection, and diffusion.

Reactor type	Mechanisms[a]	Consideration of kinetics				Mass transport description[b]	Solution method	Reference
		Substrate in bulk phase	Substrate in biofilm	Biofilm amount	Substrate in GAC			
Complex mixing	A, B	Nonsteady Monod	Monod	Nonsteady	Non-equilibrium	1, 2, 3, 4, 5	Analytical	Chang and Rittmann [14]
Column	A, B, C, D	Nonsteady, no biodegradation, uniform Monod	n.a.[c]	Steady	Equilibrium	1	Analytical	Sakoda, Wang and Suzuki [17]

Reactor type	Mechanisms[a]	Consideration of kinetics				Mass transport description[b]	Solution method	Reference
		Substrate in bulk phase	Substrate in biofilm	Biofilm amount	Substrate in GAC			
Column	A, B	Uniform	Monod	Nonsteady	n.a.[c]	1	Analytical	Walker and Weatherley [18]
Column	A, B, C	Nonsteady, no biodegradation	Monod	Steady	Non-equilibrium	1, 5	Analytical	Abumaizar, Smith and Kocher [19]
Column	B, C, D	Nonsteady Monod	Monod	Nonsteady	n.a.[c]	1, 2, 3	Numerical	Hozalski and Bouwer [20]
Column	A, B, C, D	Nonsteady, no biodegradation	Monod	Nonsteady	Non-equilibrium	1, 2, 3, 4, 5	Numerical	Badriyha, Ravindran, Den and Pirbazari [21]
Column	A, B, C, D	Nonsteady, no biodegradation, uniform Monod	Monod	Steady	Non-equilibrium	1, 2, 3, 4, 5	Numerical	Liang and Chiang [15]

[a]A, adsorption; B, biodegradation; C, convection; D, dispersion.

[b]1, bulk phase; 2, interface between bulk phase and biofilm; 3, biofilm; 4, interface between biofilm and GAC; 5, GAC.

[c]Not analyzed in the article.

Table 3. Several representative models for biological activated carbon (BAC) process (modified from Liang et al. [16])

3.1.2. Non-steady-state models for adsorption and biodegradation of BAC

A numerical model can be developed to simulate both adsorption and biodegradation quantities of a BAC column under a non-steady-state condition. The governing equation based on mass balance of the substrate concentration in the liquid phase of the BAC column can be expressed as follows [16]:

$$\varepsilon \frac{\partial S_b}{\partial t} = D_b \frac{\partial^2 S_b}{\partial x^2} - v\frac{\partial S_b}{\partial x} - \frac{(1-\varepsilon)}{V_g}\int_0^{L_f} \frac{k_f X_f S_f}{K_f + S_f} 4\pi \left(r_f + r_g\right)^2 dr_f - (1-\varepsilon)\rho_g \frac{\partial q_a}{\partial t} - \varepsilon\left(\frac{k_b X_b S_b}{K_b + S_b}\right) \quad (20)$$

http://dx.doi.org/10.5772/60917

Table 4 presents the parameter details of Equation (20):

Abbreviations	Units	Descriptions
ε	-	Bed porosity of the BAC column
S_b	M/L^3	Substrate concentration in the liquid phase
D_b	L^2/T	Dispersion coefficient in the liquid phase
x	L	Distance along the BAC column
V_g	L^3	Volume of a GAC granule
L_f	L	Length of the biofilm
k_f	M/T-cell	Maximum utilization rate in the biofilm
k_b	M/T-cell	Maximum utilization rate in the liquid phase
X_f	cell/L^3	Cell density of the biofilm
X_b	cell/L^3	Cell density in the liquid phase
S_f	M/L^3	Substrate concentration in the biofilm
K_f	M/L^3	Monod half-velocity coefficient in the biofilm
K_b	M/L^3	Monod half-velocity coefficient in the liquid phase
r_f	L	Radius of the biofilm
r_g	L	Radius of the GAC granule
ϱ_g	M/L^3	GAC granule apparent density
q_a	M/M	Adsorption capacity

Table 4. Parameter details of non-steady-state models for adsorption and biodegradation of BAC

Two boundary conditions (BC) for the equation of dispersion advection reaction can be described as follows:

$$\mathrm{BC1}: S_b = S_0 \ , \ \ x = 0, \ \text{and} \ \ t \geq 0 \tag{21}$$

$$\mathrm{BC2}: \frac{\partial S_b}{\partial x} = 0 \Big|_{x=L_c} \tag{22}$$

where Lc is the length of the BAC column (L). If the diffusion and reaction simultaneously occurred under a non-steady-state biofilm condition, the non-steady-state form of mass transfer and biodegradation reaction within biofilm, based on Fick's law and Monod equation, can be expressed as

$$\frac{\partial S_f}{\partial t} = D_f \frac{\partial^2 S_f}{\partial r_f^2} - \frac{k_f S_f}{K_s + S_f} X_f \qquad 0 \le r_f \le L_f \tag{23}$$

where D_f (L^2/T) is the diffusivity within the biofilm. A diffusion layer exists between the bulk solution and the biofilm, and the substrate concentration profile can be solved according to Rittmann and McCarty [22]. Therefore, the boundary condition can be simplified as

$$S_f\big|_{r_f=0} = k_{bf} S_b \tag{24}$$

where k_{bf} is a factor to estimate the concentration reduction within the diffusion layer. Langmuir isotherm was used for the calculation of the boundary concentration of the biofilm near the GAC side, which was derived from the solid-phase concentration of the adsorbates. For single-component adsorbate, the surface concentration (q_s, M/M) can be expressed as follows:

$$q_s = \frac{q_0 K_L C_a}{1 + K_L C_a} \tag{25}$$

where q_0 (M/M) is the unit layer adsorption capacity, K_L (L^3/M) is the Langmuir coefficient, and C_a (M/L^3) is the concentration on the boundary of the biofilm. It is assumed that the concentration flux from the biofilm should be identical to the substrate absorbed on a GAC granule, as Equation (26):

$$4\pi r_g^2 \cdot D_f \left.\frac{\partial S_f}{\partial r_f}\right|_{r_f = L_f} = \frac{\partial q_a}{\partial t} m_g \tag{26}$$

where m_g (M) is the mass of a GAC granule. In a control volume, the average biodegradation rate can be derived by integrating the Monod reaction expression and the amount of biofilm volume:

$$\left[\int_0^{L_f} \frac{k_f S_f}{K_f + S_f} X_f 4\pi \left(r_g + r_f\right)^2 dr_f\right] \times N_g \qquad 0 \le r_f \le L_f \tag{27}$$

$$N_g = \frac{\Delta V \left(1 - \varepsilon\right)}{V_g} \tag{28}$$

where ΔV is a control volume unit of the BAC bed (L^3) and Ng is the number of BAC granules in a control volume.

http://dx.doi.org/10.5772/60917

3.1.3. Estimation of biofilm thickness

On the other hand, the thickness of biofilm will increase due to growth and decrease by the shear of water and the self-decay of bacteria. As a result, the biofilm thickness can be described as

$$\frac{\partial L_f}{\partial t} = \frac{Y\int_0^{L_f} \frac{kS_f}{K_s + S_f} X_f 4\pi\left(r_g + r_f\right)^2 dr_f}{A_f X_f} - b_{tot} L_f, \quad 0 \le r_f \le L_f \tag{29}$$

where Y is the yield coefficient of biomass (CFU/M) and A_f is the surface area of a BAC granule (L^2).

In addition, the governing equation for the bacterial density in bulk solution can be simplified as an advection–reaction form:

$$\frac{\partial X_b}{\partial t} = -v\frac{\partial X_s}{\partial x} + \frac{Yk_b S_b X_b}{K_b + S_b} \tag{30}$$

In this situation, the BCs of Equation (30) can be expressed as follows:

$$\text{BC1}: X_b = S_0 \quad x = 0, \ t \ge 0 \tag{31}$$

$$\text{BC2}: \frac{\partial S_b}{\partial x} = 0\Big|_{x=L_c} \tag{32}$$

The governing equation is a second-order partial-differential equation, which can be approximately solved by the Crank–Nicolson finite differential and Crout factorization methods. Therefore, the developed model can quantify the amounts of adsorption and biodegradation. In addition, the significances of each parameter can be determined throughout the results of sensitivity analysis.

3.2. Engineering practice

3.2.1. Dimensionless analysis

The mass transfer coefficient can be determined by the dimensionless groups of Reynolds (Re), Sherwood (Sh), and Schmidt (Sc) numbers. Since these dimensionless groups are developed for process scale-up, different reactors can be compared to each other through the dimensionless analysis. The Reynolds number represents the ratio between inertial force and viscous

force, and the Sherwood number represents the ratio between liquid-film transfer and biofilm diffusive transfer. The N_{Sh} can be correlated with the dimensionless groups as follows (Wakao and Funazkri, 1978):

$$N_{Sh} = 2 + 1.1 \times N_{Re}^{1/2} N_{Sc}^{1/3} \tag{33}$$

Several key operational parameters reasonably dominating the performance of a BAC column include the superficial influent velocity and the particle size of packing. As a result, the effects of particle size on adsorption and biodegradation can be simulated by the dimensional analysis.

3.2.2. Liquid-film mass transfer

Figure 5 shows the relationship between the Stanton number (N_{St}) and the liquid-phase mass transfer coefficient ($k_b f$) reported in the literature. It is observed that the Stanton number (i.e., the ratio of the liquid-film transfer to the bulk transfer) exhibits an inverse proportion to the particle size (d_p) and the superficial velocity (v_s). In other words, both larger particle sizes and higher superficial velocities will lead to a relatively lower performance in liquid-film mass transfer (N_{St}). Therefore, the mass transfer from bulk solution into the biofilm can be enhanced with the increase of the Stanton number.

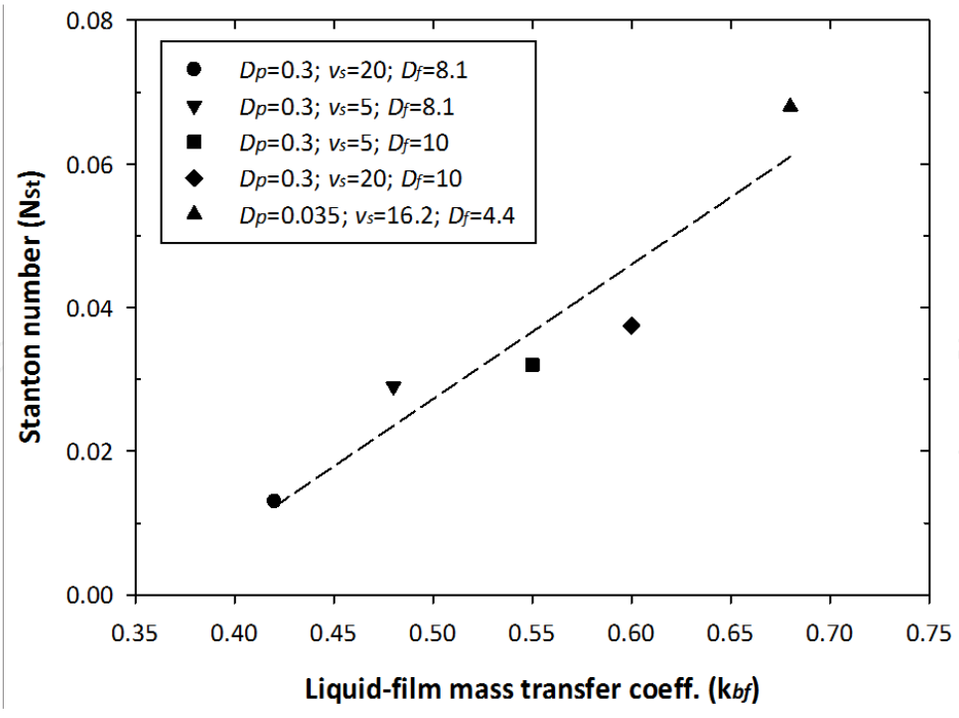

Figure 5. Correlation between the Stanton number (N_{St}) and the liquid-film mass transfer coefficient (k_{bf}). D_p (cm) is the particle size, v_s (cm/min) is the superficial velocity, and D_f (10^{-6} cm^2/s) is the diffusivity. Available data was from Liang et al. [16]) and Badriyha et al. [21])

http://dx.doi.org/10.5772/60917

4. Chlorination process

4.1. Model development

Chlorination (using chlorine as disinfectant) is the common process used in daily water disinfection because of its high efficiency with a relatively low cost. However, as aforementioned in the Ozonation chapter, the disinfection by-products (DBP), specifically trihalomethane (THM) including chloroform, bromodichloromethane, dibromochloromethane, and bromoform, will also be formed during the chlorination process. Control of the formation potential of THM during chlorination is thus an important target for the supply of drinking water. THMs can be formed in the presence of specific precursors such as humic substances and methyl ketones [23]. Several good engineering practices to prevent THM formation include (1) decrease of chlorine dose, (2) change of the point of chlorination, (3) substitution with an alternative disinfectant, and (4) reduction of precursors in solution by GAC or enhanced coagulation. In addition, several factors including precursor concentration (as represented by total organic carbon concentration), chlorine dose, bromide concentration, reaction temperature, pH of solution, contact time, and reactor configuration (length-to-width ratio and mixing conditions) will affect the formation of THMs. To predict the performance of disinfection efficiency and kinetics, and/or THM formation potential, numerous models such as dispersion model have been applied in chlorine process, as illustrated in the following context.

4.1.1. Dispersion model

In general, the chlorination process is applied in either a rectangular basin with baffles (rectangular-long and narrow channel) or a circular basin (circular-annular ring surrounding). The hydrology in a rectangular basin with baffles is the most advantageous because of a plug-flow-like reactor. It can be examined by the exit age distribution (E_θ) curve (Equation (34)) of the basin reactor, assuming the independence of fluid element and agitation with respect to radial position [24]:

$$E_\theta = \frac{1}{\sqrt{4\pi\theta d}} exp \frac{-(1-\theta)^2}{4\theta d} \tag{34}$$

where d is the dimensionless diffusion coefficient representing the degree of axial mixing. The d value approaching zero represents the reactor behaving as an ideal plug-flow type, otherwise (approaches infinity) representing a mixed-flow type. The E_θ in Equation (34) is a function of θ which follows a Gaussian distribution.

For a baffled rectangular basin with a total flow length of L and a channel width of W, the dimensionless diffusion coefficient (d) in open-channel flow, taking the nonideal nature of the reactor into consideration, could be expressed by Equation (35) [25]:

$$d = \frac{0.14k}{L/W} \tag{35}$$

where k is a nonideality coefficient of the reactor.

4.1.2. Disinfection kinetics

According to Collins and Selleck [26], the die-off of microorganisms in a batch reactor due to disinfection can be expressed by Equations (36) and (37):

$$\left[\frac{N}{N_0}\right]_{\text{batch}} = 1, \quad \text{for } \theta < \frac{b}{CT} \tag{36}$$

$$\left[\frac{N}{N_0}\right]_{\text{batch}} = \left(\frac{b}{Ct}\right)^n, \text{ for } \theta < \frac{b}{CT} \tag{37}$$

where t is the exit residence time representing the actual traveling time of the component of the fluid. The value of b for the combined chlorine was about 4 and 2.8 for total coliform and fecal coliform, respectively, and the value of n was about 3 for both total and fecal coliform [26]. T is the theoretical residence time (i.e., hydraulic retention time (HRT)), measured as the volume divided by the flow rate.

The overall survival fraction of bacteria can be determined by integrating the survival fraction of a series of batch reactors over the E_θ function, if the reaction in a continuous flow reactor. In this case, the average disinfection efficiency (i.e., 1 – (N/No)) is expressed as follows [25]:

$$1 - \frac{N}{N_0} = 1 - \int_0^\infty \left[\frac{N}{N_0}\right]_{\text{batch}} E_\theta d\theta \tag{38}$$

Therefore, the average disinfection efficiency can be calculated by the given chlorine dose (C), dimensionless diffusion coefficient (d), disinfection coefficients (b and n), and residence time distribution function (E_θ and $d\theta$) using Equation (39) [25]:

$$\begin{aligned} 1 - \int_0^\infty \left[\frac{N}{N_0}\right]_{\text{batch}} E_\theta d\theta = 1 - & \int_0^{b/CT} \frac{1}{\sqrt{4\pi\theta d}} \exp\left(\frac{-(1-\theta)^2}{4\theta d}\right) d\theta \\ & + \int_{b/CT}^\infty \left(\frac{b}{CT}\right)^n \frac{1}{\sqrt{4\pi\theta d}} \exp\left(\frac{-(1-\theta)^2}{4\theta d}\right) d\theta \end{aligned} \tag{39}$$

http://dx.doi.org/10.5772/60917

4.1.3. Formation kinetics of THMs

The reaction chemistry between chlorine and aquatic humic precursors to form THMs can be expressed by the following short-hand way [25]:

$$Cl_2 + m''\,\mathrm{TOC}\left(\text{precursors}\right) \rightarrow \mathrm{THMs} + \text{other products} \tag{40}$$

Based on the above process chemistry, the kinetics of chlorine decay and the THMs formation can be expressed by Equations (41) and (42), respectively:

$$-\frac{d\left[Cl_2\right]}{dt} = k_1\left[Cl_2\right]\left[\mathrm{TOC}\right]^{m'} \tag{41}$$

$$\frac{d\left[\mathrm{THMs}\right]}{dt} = k_2\left[Cl_2\right]\left[\mathrm{TOC}\right]^{m} \tag{42}$$

When reactions take place in a continuous flow reactor, the overall change of free chlorine and THMs can be obtained by integration of the batch concentration over the entire exit time distribution (E_θ) as follows:

$$\begin{aligned}\left(\frac{\left[Cl_2\right]}{\left[Cl_2\right]_0}\right) &= \int_0^\infty \left(\frac{\left[Cl_2\right]}{\left[Cl_2\right]_0}\right)_{\mathrm{batch}} E_\theta d\theta = \\ &= \int_0^\infty \frac{1}{\sqrt{4\pi\theta d}} \exp\left(\frac{-\left(1-\theta\right)^2}{4\theta d}\right) \exp\left(-k_1 T\theta\left[\mathrm{TOC}\right]\right) d\theta\end{aligned} \tag{43}$$

$$\begin{aligned}[\mathrm{THMs}] &= \int_0^\infty [\mathrm{THMs}]_{\mathrm{batch}} E_\theta d\theta = \\ &= \int_0^\infty k_2 T\left[TOC\right]^m \left[Cl_2\right]_0 \exp(-k_1 T\theta[\mathrm{TOC}]) \frac{1}{\sqrt{4\pi\theta d}} \exp\left(\frac{-\left(1-\theta\right)^2}{4\theta d}\right) d\theta\end{aligned} \tag{44}$$

4.2. Engineering practice

4.2.1. Determination of coefficients in disinfection kinetic model

In practice, the total coliform and total bacteria count can be measured by the membrane filter method and heterotrophic plate count method, respectively. The effect of chlorine doses and contact time on the survival of total coliform and total bacteria can be determined, as shown in Figures 6 (a) and (b), respectively.

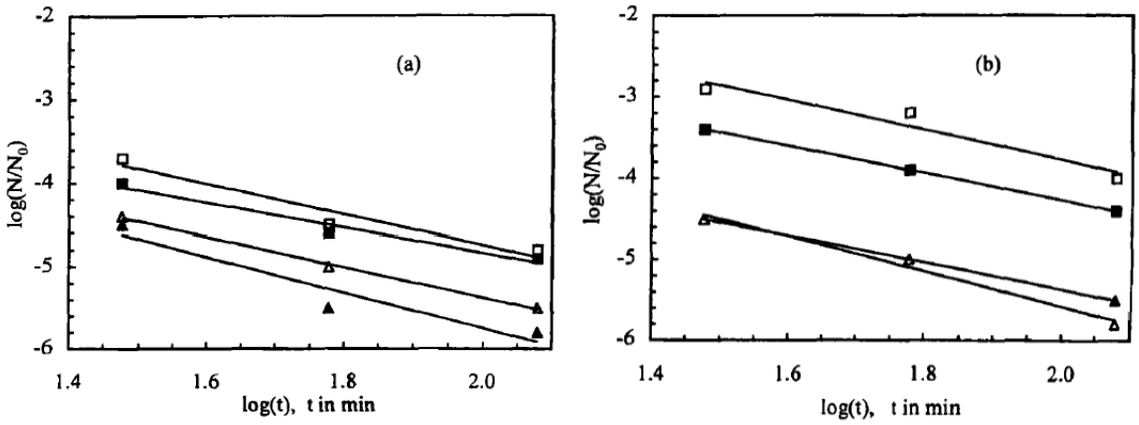

Figure 6. Effect of applied chlorine and contact time on survival of (a) total coliform and (b) total count. □ Cl_2, 1.2 mg/L; ■ Cl_2, 2.0 mg/L; ΔCl_2, 1.8 mg/L; ▲Cl_2, 0.9 mg/L. (Adapted from Chiang et al. [25])

4.2.2. Prediction of THMs Formation

As shown in Figure 7, the effect of the contact time (i.e., 0–70 min) and the chlorine dose (i.e., 0.5–8.0 mg/L) on the THM formation was presented at a TOC of 3 mg/L with an L/W ratio of 20. The THM concentrations increase linearly with the contact time over the range of 0 to 70 min. By knowing the water quality parameters and experimental conditions, it is possible to predict the THM formation in the effluent of the chlorine contact chamber. To keep the THM formation below 100 μg/L at the water treatment plant, it is necessary to maintain the chlorine dose below 2 mg/L for a contact basin with an L/W ratio of 20.

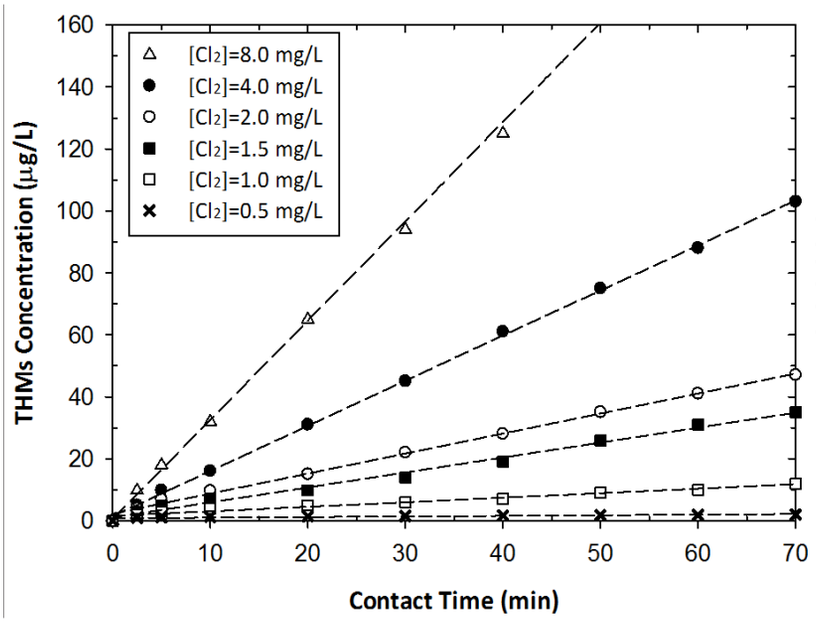

Figure 7. Effect of applied chlorine dose ad contact time on THM formation at inlet TOC concentration of 3.0 mg/L and an L/W ratio of 20. (Modified from Chiang et al. [25])

4.2.3. Balancing disinfection efficiency and THM formation

As the aforementioned, balancing the disinfection efficiency (in Section 2.1) and THM formation (in Section 2.2) is an important task in chlorination process. Table 5 provides the engineering practice (exemplified by Case A wastewater treatment plant) to balance the disinfection efficiencies and THM formation, in terms of contact time, L/W ratio, and applied chlorine doses. It can be used to determine the applied chlorine dose needed to meet a specified degree of inactivation (e.g., 99.99 % kill) and level of THM formation. In general, the THM formation increases rapidly with the increases of contact time. Conversely, the disinfection efficiency of chlorine increases gradually as both contact time and chlorine dosage increase.

It is noted that the applied chlorine dose at about 1.0 mg/L exhibits the most economically feasible way to control the THM formation and to maintain the disinfection efficiency at the Case A water treatment plant. Under these conditions, the Case A plant is able to achieve an acceptable level of residual chlorine (i.e., 0.5 mg/L) at the THM formation below 100 μg/L.

Items		**Unit**	**Category I**			**Category II**			**Category III**		
Applied chlorine		mg/L	0.5	0.5	0.5	1.0	1.0	1.0	1.25	1.25	1.25
L/W		–	2	10	20	2	10	20	2	10	20
Disinfection efficiency	20 min	%	99.40	99.59	99.62	99.96	99.97	99.98	99.98	99.98	99.99
	30 min	%	99.94	99.96	99.96	99.98	99.99	99.99	99.99	99.99	99.99
	40 min	%	99.97	99.98	99.98	99.99	99.99	99.99	99.99	99.99	99.99
	50 min	%	99.98	99.99	99.99	99.99	99.99	99.99	99.99	99.99	99.99
THM formation	20 min	μg/L	3.54	3.99	4.00	7.08	7.97	7.99	8.85	9.97	9.99
	30 min	μg/L	5.22	5.90	5.91	10.45	11.79	11.83	13.06	14.74	14.79
	40 min	μg/L	6.85	7.75	7.78	13.70	15.50	15.56	17.13	19.37	19.45
	50 min	μg/L	8.42	9.55	9.60	16.85	19.10	19.20	21.06	23.88	23.99

Table 5. Disinfection efficiency and THM formation during chlorination at TOC = 3 mg/L in a real water treatment plant (Case A) (modified from Chiang et al. [25])

In addition, the THM concentration and disinfection efficiency associated with a given contact time, L/W ratio, and applied chlorine dose are also presented in Table 5. Prior to chlorine input to the solution, reducing the TOC concentration is definitely the best engineering practice (BEP) for controlling the THM formation, rather than improving the hydraulics through the geometric design of the reactor. On the other hand, the results imply that the geometry of a chlorine contactor can effectively control the disinfection efficiency (not on the formation of THMs), especially for large chlorine doses and a high L/W ratio.

Furthermore, in order to reduce the formation of THM, the ozonation process is sometimes utilized in disinfection for the purpose of eliminating bacteria, viruses, cysts, as well as organic compounds, especially, the precursors of disinfection DBPs [27]. The performance of the ozone

disinfection processes is evaluated by the residual ozone and contact time. Therefore, factors such as the efficiency of gas–liquid contact, chemical reactivity of the raw water toward ozone, susceptibility of microorganisms, and hydrodynamic characteristics of the contactor can influence the disinfection performance of an ozonation process. Several researchers have shown that ozonation prior to chlorination can lower the formation potential of THM (trihalomethanes) and HAA (haloacetic acid) [28, 29].

5. Carbonation process

5.1. Model development

5.1.1. Process chemistry

Carbonation is generally classified as a heterogeneous reaction containing gas, liquid, and solid phases. CO_2 fixation by accelerated carbonation has been regarded as mass transfer limited reaction (i.e., film-diffusion controlled) according to the findings reported in the literature [30-32]. Therefore, different types of approaches such as physical intensification [33] and biological or chemical activation [34, 35] were recently carried out to improve the mass transfer and reaction kinetics. Based on this idea, a rotating packed bed (RPB) reactor has been introduced to improve the mass transfer rate among phases due to its high centrifugal forces and great micro-mixing ability. RPB, the so-called high-gravity (sometimes called the "HI-GEE") process, is able to generate high acceleration via centrifugal force so the mass transfer between gas and liquid and even between liquid and solid can be enhanced. Since RPB can provide a mean acceleration of hundreds, and even thousands, of times greater than the force of gravity, it can effectively lead to the formation of thin liquid films and micro- or nano-droplets [36-38]. Therefore, the volumetric gas–liquid mass transfer coefficients ($K_G a$) are an order of magnitude higher than those in a conventional packed bed, leading to dramatic reductions in equipment size over that required for equivalent mass transfer in a gravity-flow packed bed [36, 38, 39].

According to the findings in the literature [40], the CO_2 consumption in bulk solution was mainly attributed (over 98 % contribution) to carbonation reaction with calcium ions in solution leached from the steel slag to form calcium carbonate precipitates, where the stoichiometric formula was briefly presented as Equation (45). In this case, the stoichiometric coefficient (b) is assigned a value of one.

$$CO_{2(\text{fluid})} + b\ CaO_{(\text{solid})} \rightarrow CaCO_{3(s)} \tag{45}$$

From the gas-phase point of view, the CO_2 removal efficiency (η) for a carbonation process can be calculated as Equation (46):

$$\eta\left(\%\right) = \left[1 - \frac{\left(\rho_{CO_2,o} Q_{G,o}\ C_{G,o}\right)}{\rho_{CO_2,i} Q_{G,i}\ C_{G,i}}\right] \times \% \tag{46}$$

http://dx.doi.org/10.5772/60917

where the $\rho_{CO_2,i}$ and $\rho_{CO_2,o}$ are the densities of inflow and outflow streams of CO_2, respectively. $Q_{G,i}$ and $Q_{G,o}$ are the flow rates of inflow and outflow streams, respectively. $C_{G,i}$ and $C_{G,o}$ are the CO_2 concentration in inflow and outflow streams, respectively.

From the solid-phase point of view, the carbonation conversion (X_B, %) of the solid can be defined as the ratio of reacted CaO fraction with CO_2 to the original total available CaO content in solid before carbonation., as expressed in Equation (47):

$$X_B(\%) = \left[\frac{\Delta m_{CO_2}}{MW_{CO_2}} \times \frac{MW_{Cao}}{CaO_{total}}\right] \times \% \quad (47)$$

where Δm_{CO2} is the weight gain due to CO_2 carbonation per dry weight of the solid sample. MW_{CaO} and MW_{CO2} are the molecular weight of CaO and CO_2, respectively. CaO_{total} is the total available CaO content in the solid before carbonation.

5.1.2. Rate-determining steps

The shrinking core model (SCM) has been utilized to determine the rate-limiting steps in a heterogeneous reaction because of its conceptual and mathematical simplicity [41]. In the SCM, it is assumed that the reaction occurs at the outer skin of solid particle and then proceeds at a narrow front [24]. The narrow front moves into the particle and leaves behind completely reacted product layer and/or reactive-species-depleted rims (i.e., ash layer). An unreacted core of material exists at any time, which shrinks in size during the reaction. Based on the above assumption, three factors might affect the reaction (i.e., rate-limiting steps) including (1) fluid-film diffusion, (2) ash-layer (or product layer) diffusion, and (3) chemical reaction at the unreacted-core surface, as illustrated in Figure 8.

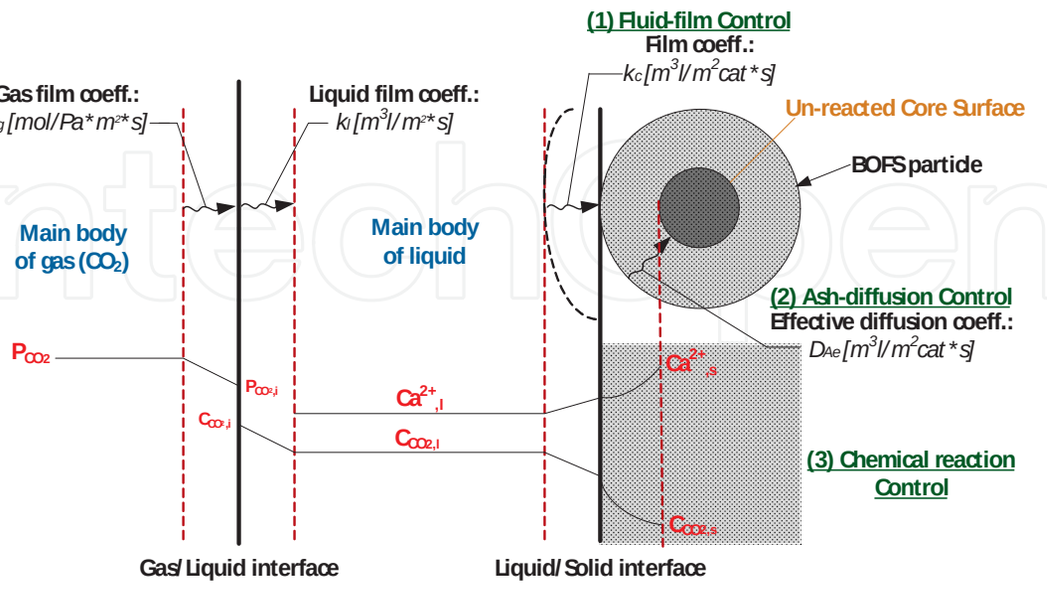

Figure 8. Schematic diagram of mass transfer among gas, liquid, and solid phases in the case of basic oxygen furnace slag (BOFS) carbonation.

When the reactant transfer through the boundary layer of the liquid–solid interface is the rate-limiting step of a reaction, the relationship between the conversion (X_B, %) and reaction time (t, s) can be correlated with Equation (48):

$$t = \frac{\rho_B R}{3bk_e C_{Ag}} X_B = \tau\ X_B \tag{48}$$

where ρ_B (mole cm^{-3}) and R (cm) are the molar density and the radius of the particle, respectively, C_{Ag} (mole cm^{-3}) is the CO_2 concentration in the liquid phase, k_e (mole m^{-2} Pa^{-1} s^{-1}) is the mass transfer coefficient between the fluid and particle, and τ (s) is the time for complete conversion to a product particle.

When the reactant transfer through the ash layer is the rate-limiting step, the dependence of the reaction time on the conversion and the effective diffusivity of the reactant in the ash layer (D_e, cm^2 s^{-1}) can be described by Equation (49):

$$t = \frac{\rho_B R^2}{6bD_e C_{Ag}}\left[1-3\left(1-X_B\right)^{2/3}+2\left(1-X_B\right)\right] = \tau\left[1-3\left(1-X_B\right)^{2/3}+2\left(1-X_B\right)\right] \tag{49}$$

For simplicity, the particle radius (R) is generally assumed to remain constant in the literature. However, in reality, the R value is not a constant because the thickness of ash layer changes with the reaction, also affecting the diffusivity of the gaseous reactant in the ash layer. Sohn and Szekely [42] have introduced this phenomenon into SCM to make it more general to the fluid–solid reaction. In their recent report [43], a "Z" factor was incorporated with the governing equation of SCM for pore diffusion control, as shown in Equation (50). Z is defined as the volume of product solid formed from a unit volume of reactant solid, where both volumes include those of pores. In this case, the volume of the solid product is different from that of the solid reactant, which means R changes with time:

$$t = \frac{\rho_B R^2}{2bD_e C_{Ag}}\left[\frac{Z-\left(Z-\left(Z-1\right)\left(1-X_B\right)\right)^{2/3}}{Z-1}-\left(1-X_B\right)^{2/3}\right] \tag{50}$$

If the R value is assumed to remain constant, the Z, herein, should be assigned a value of 1, i.e., the total volume of solid product is the same as that of solid reactant. Thus, Equation (50) will be simplified to Equation (49) by applying L'Hospital's rule.

When the chemical reaction between reactants is the rate-limiting step, the relationship between the conversion and reaction time can be determined by Equation (51):

$$t = \frac{\rho_B R}{bk'' C_{Ag}}\left[1-\left(1-X_B\right)^{1/3}\right] = \tau\left[1-\left(1-X_B\right)^{1/3}\right] \tag{51}$$

where k'' (s^{-1}) is the first-order rate constant for the surface reaction.

http://dx.doi.org/10.5772/60917

5.1.3. Mass transfer coefficients

For determining the $K_G a$ value in a heterogeneous system containing the gas, liquid, and solid phases, the following assumptions are generally made for simplicity: (1) the effect of an inclined gas–liquid interface is neglected, (2) solid distribution throughout the bed is uniform, (3) the concentration of the liquid at the particle surface is equal to the saturation concentration of the solution (i.e., the mass transfer between the liquid and the solid is neglected), and (4) the changes in particle size and particle surface area are neglected. In this case, the $K_G a$ in a packed bed can be determined by the two-film theory as Equation (52):

$$\frac{1}{K_G a_e} = \frac{1}{k_G a_e} + \frac{H}{I(k_L a_e)} \tag{52}$$

where k_G is the gas-side mass transfer coefficient (m s^{-1}), k_L is the liquid-side mass transfer coefficient (m s^{-1}), H is the Henry's law constant, and I is the enhancement factor.

On the other hand, the driving force between the saturated CO_2 concentration in the bulk gas and the CO_2 concentration on the surface of liquid film can be determined by shell mass balance over a thin film of fluid with the RPB as shown in Equations (53) and (54):

$$\frac{1}{\rho_{CO_2}} \frac{\mathrm{d}M_G}{\mathrm{d}V} = K_G a_e \ (C_G^* - C_G^{'}) \tag{53}$$

$$\mathrm{d}V = 2\pi r h \cdot \mathrm{d}r \tag{54}$$

where ϱ_{co2} is the CO_2 mass density at the temperature of gas streams, M_G is the gas mass flow rate (kg s^{-1}), C_G^* is the saturation concentration of CO_2 in solution (mg/L), $C_G^{'}$ is the concentration of CO_2 in solution (mg/L), V is the volume of packed bed (m^3), h is the height of packing bed (m), and r is the radius of packed bed (m).

In this case, by substitution of Equation (54) into Equation (53), the $K_G a$ can be determined as Equation (55):

$$K_G a_e = \frac{M_G}{\rho_G h\pi (r_o^2 - r_i^2)} \left(NTU_G\right) = \frac{Q_G}{h\pi (r_o^2 - r_i^2)} ln\left(\frac{C_{G,i}}{C_{G,o}}\right) \tag{55}$$

Furthermore, Kelleher and Fair (1996) have obtained an overall volumetric mass transfer coefficient in terms of the area of transfer unit (ATU) for the gas side from the literature [44]. The height of transfer unit (HTU) and ATU can be calculated from the experimental data using Equations (56) and (57), respectively [45]:

$$\mathrm{HTU} = \frac{r_o - r_i}{\mathrm{NTU}} = \frac{r_o - r_i}{\ln(C_{G,i} / C_{G,o})} \tag{56}$$

$$\mathrm{ATU} = \frac{\pi (r_o^2 - r_i^2)}{\mathrm{NTU}} = \frac{\pi (r_o^2 - r_i^2)}{\ln(C_{G,i} / C_{G,o})} \tag{57}$$

It is noted that the $K_G a$ value in an RPB are an order of magnitude greater than those in a conventional packed bed. In other words, the HTU value of an RPB is smaller than that of conventional packed bed. Therefore, the volume of the RPB reactor for achieving a certain degree of performance is much smaller than that of a conventional reactor such as autoclave and slurry reactors [38, 39]. Several operating factors will affect the performance of RPB reactor. In general, $K_G a$ increases with the increases of the gas flow rate, the liquid flow rate, and mainly the rotor speed [46].

5.2. Engineering practice

5.2.1. Determination of diffusion coefficients

According to the findings reported by Changet al. [47], the accelerated carbonation of the basic oxygen furnace slag (BOFS) in an RPB is controlled by the ash-layer diffusion mechanism because the experimental data exhibit a good correlation with Equation (51). Similar findings were observed in the literature [48], which suggests that the carbonation reaction should be ash-layer diffusion controlled. The particles exhibited an ash layer of calcium carbonate ($CaCO_3$) product after carbonation, which could be classified as a shrinking core. As shown in Figure 9, the D_e values of CO_2 gas through the ash layer are in the range of 5.47×10^{-7} to 1.49×10^{-6} cm^2 s^{-1}, increasing with the increase of reaction temperature.

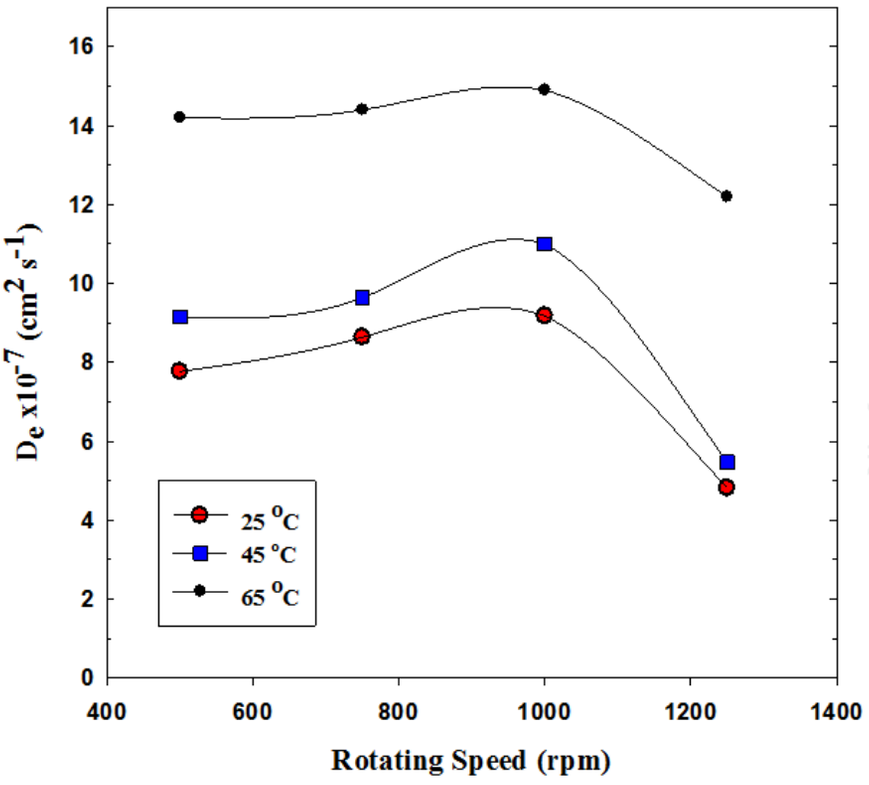

Figure 9. Variation of D_e with reaction temperature for BOFS carbonation based on the SCM (operating conditions: P_{CO2}, 1 bar; flow rate, 1.2 L min^{-1}; D_p, ~ 62 μm; L/S, 20 mL/g^{-1}) (adapted from Chang et al. [47])

http://dx.doi.org/10.5772/60917

In addition, Changet al. [41]) reported an effective diffusivity of steelmaking slag in a slurry reactor of 2.9×10^{-7} to 7.3×10^{-7} $cm^2\ s^{-1}$ according to the results of the SCM. It was found that the rate of CO_2 molecular diffusion was not significantly enhanced by the RPB because the very similar temperatures were operated in the two reactors. Therefore, the D_e values measured in a slurry reactor exhibit the same magnitude of 10^{-6} $cm^2\ s^{-1}$ to that in an RPB. Equation (58) shows the relationship between D_e value ($L^2\ T^{-1}$) and K_Ga (L T^{-1}) value:

$$K_G = \frac{D_e}{\delta} \tag{58}$$

where δ (L) is the thickness of fluid film. Only a slight discrepancy in *De* values between an RPB and a slurry reactor was found; however, the RPB reactor can generate a thinner liquid film (δ), thereby resulting in a higher mass transfer rate.

5.2.2. Determination of overall gas-phase mass transfer coefficients

Based on the above illustration, the K_Ga value in an RPB can be estimated by the key operating parameters including gas diffusivity, gas superficial velocity, gas density, gas viscosity, liquid superficial velocity, liquid density, liquid viscosity, centrifugal acceleration, total specific surface area of packings, and effective diameter of packings. Therefore, the mass transfer characteristics of RPB (such as K_Ga value and HTU) can be obtained by the nonlinear regression of experimental data [49]:

$$K_Ga_e = 0.01\left(\frac{a_tD_G}{d_p}\right) Re_G^{-1.16}\ Gr_G^{0.33}\ Re_L^{2.12} \tag{59}$$

$$HTU = 0.0003\left(\frac{a_tD_G}{d_p}\right) Re_G^{2.16}\ Gr_G^{-0.33}\ Re_L^{-2.12} \tag{60}$$

where the ranges of the dimensionless groups in this correlation should be as follows:

$$7.8 < Re_G < 15.9 \tag{61}$$

$$1.3 < Re_L < 2.2 \tag{62}$$

$$2.3 < Gr_G < 26.8 \tag{63}$$

Table 6 presents the K_Ga value for high-gravity carbonation of BOFS-CRW, respectively. The rotation speed varied from 150 to 550 rpm, offering a centrifugal acceleration variation from

60 m/s^2 to 770 m/s^2. The K_Ga values moderately increase with an increase of rotation speed (i.e., up to 300–500 rpm), indicating that the mass transfer resistance was reduced by an increasing rotation speed within this range. However, a reduction in K_Ga was observed if the rotation speed further increased beyond this range. This might be attributed to the fact that the extent of reduction in mass transfer resistances at higher rotation speed was compensated for by a reduction of the retention time, which was unfavorable to reaction.

No	ω'a (rpm)	Q_G [a] (m^3/min)	Q_{sl} [a] (L/min)	G/L ratio (-)	L/S ratio (mL/g)	K_Ga value (s^{-1})
1	462.1	0.33	9.33	35.4	10.12	0.672
2	462.7	0.34	9.33	36.4	10.61	0.650
3	505.1	0.82	6.50	126.2	12.35	0.715
4	487.3	0.44	9.17	48.0	11.21	0.680
5	534.4	0.72	6.33	113.7	12.77	0.632
6	360.2	0.42	9.00	46.7	10.06	0.699

[a]ω', rotation speed (rpm); Q_G, gas flow rate (m^3/min); Q_{sl}, slurry flow rate (L/min)

Table 6. Candidates of optimal K_Ga solutions under different operating conditions and verified with theoretical model

On the other hand, several studies have utilized different kinetic models to determine the rate-limiting step of mineral carbonation [31, 41]. In fact, solid–liquid mass transfer is particularly important in mineral carbonation and, in many cases, the rate limiting factor [50, 51] because minerals in solid matrix dissolve partly and passive layers are formed, gradually increasing resistance to mass transfer and eventually leading to incomplete conversion. In general, the solid–liquid mass transfer coefficient is occasionally correlated as itself, where such correlations are specific to the system under consideration and are not generally applicable [50].

In spite of the significant differences between RPB and traditional packed column, penetration theory was still capable of describing the liquid-side mass transfer behavior fairly well in RPB [52]. These correlations are most often expressed in terms of dimensionless numbers in the form of a power series. For instance, penetration theory can be applied to RPB to yield as Equation (64):

$$k_L = 0.92 \left(\frac{D_L}{d_p} \right) Sc_L^{1/2} \, Re_L^{1/3} Gr_L^{1/6} \tag{64}$$

where the Grashof number which represents the ratio of gravitational to viscous forces can be determined by Equation (65) and the g value can be replaced by the centrifugal acceleration term as shown in Equation (66):

http://dx.doi.org/10.5772/60917

$$Gr_L = gd_p^3\left(\frac{\rho_L}{\mu_L}\right)^2 \tag{65}$$

$$g = a_m = \left(\frac{r_o^2 + r_i^2}{2}\right)^{1/2}\omega^2 \tag{66}$$

The Grashof (Gr) number is generally determined by the mean radius of the packed bed. Another commonly used prediction for liquid-side (k_L) and gas-side (k_G) mass transfer coefficient in a conventional packed column is that of Onda et al. (1968), as shown in Equations (67) and (68), respectively. Onda et al. suggested the constant 5.23 of Equation (68) should be best correlated by changing the constant into 2.00 for smaller packings (i.e., diameter is less than 1.5 cm) since the K_Ga data for packings smaller than 1.5 cm tend to decrease in the literatures [53].

$$k_L = 0.0051\left(\frac{a_t}{a_w}\right)^{2/3} Re_L^{2/3} Sc_L^{-1/2}\left(\frac{\rho_L}{\mu_L g}\right)^{-1/3}(a_p d_p)^{0.4} \tag{67}$$

and

$$k_G = 5.23\left(a_p D_G\right) Re_G^{0.7} Sc_G^{1/3}\left(a_p d_p\right)^{-2} \tag{68}$$

It is usually difficult to obtain mass transfer coefficients separated from volumetric mass transfer coefficients k_La_e and k_Ga_e since the effective interfacial area between the liquid and vapor phase is usually not known [38]. Several correlations have been reported to estimate the wetted surface area (a_w), among which Tung and Mah [52] found that the a_w/a_t predicted value by Perry and Chilton [54] is "reliable" under high-gravity RPB process as shown in Equation (69).

$$\frac{a_w}{a_t} = \frac{a_e}{a_t} = 1 - \exp[-1.45\left(\frac{\sigma_c}{\sigma_L}\right)^{0.75} Re_L^{0.1}\ We_L^{0.2}\ Fr_L^{-0.05}] \tag{69}$$

The assumption of the above equality is that for packing materials with small static holdup (i.e., large packing size), the wetted area (a_w) may equal the interfacial area (a_e). In addition, Basic (1992) has correlated the wetted surface area of packing by combining experimental data of liquid holdup and estimation of mean liquid film thickness, as shown in Equation (70):

$$\frac{a_w}{a_t} = 584\ Re_L^{-1.03}\ We_L^{0.576}\ Fr_L^{0.123} \tag{70}$$

5.2.3. Balancing mass transfer performance and energy consumption

Balancing the gas-phase mass transfer rate for the high-gravity carbonation process with a relatively lower energy consumption is also an important task for carbonation process. As shown in Figure 10, the favorable operating conditions can be determined via graphical presentation, where the energy consumptions including rotation, blowers, air compressors, and pumps were measured during operation in terms of kWh per ton CO_2 capture by the RPB. It suggests that a centrifugal acceleration should be maintained at 475 m/s^2 for a relatively lower energy consumption (L1 → L2) and higher K_Ga value (L3 → L4). Moreover, the favorable G/L ratio should range between 40 and 55 for high-gravity carbonation process (by both L5 → L6 and R1 → R2 → R3). A further increase in G/L ratio up to 80 will lead to a low mass transfer performance (i.e., K_Ga value) with high energy consumption for rotation and pumps, thereby exhibiting a poor CO_2 removal efficiency and capacity.

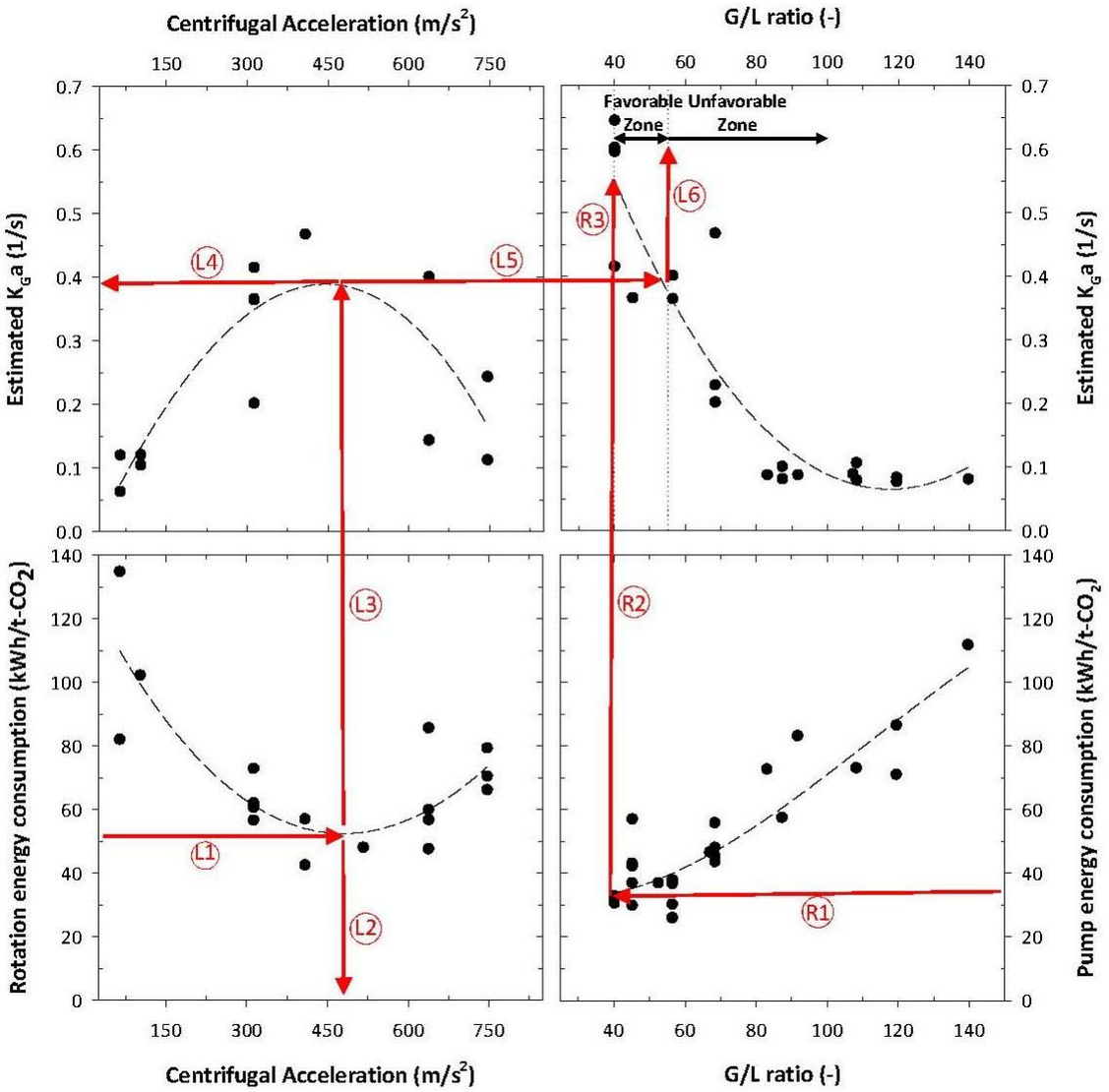

Figure 10. Graphical presentation for determining the optimal K_Ga value with favorable centrifugal acceleration (i.e., rotation speed) and G/L ratio for high-gravity carbonation process (as indicated by red line) (courtesy of Pan et al. [49])

http://dx.doi.org/10.5772/60917

6. Summary

A clear understanding in process chemistry, reaction kinetics, and mass transfer is the essential requirement to achieve the best achievable technology. Many industrial and/or waste treatment processes are involved in diffusion-controlled mechanism. To increase process efficiency and reaction rate, the mass transfer of those processes should be improved, which can be approached by development of prediction model using theoretical theory such as Fick's law or penetration theory. For those heterogeneous processes, especially the system containing gas, liquid, and solid phase, assumptions should be appropriately made to simplify the complex governing equation. Lastly, from the viewpoint of engineering practice, the energy consumption of a process is also an important factor to optimize the overall process, thereby reducing the operation costs.

Author details

Pen-Chi Chiang* and Shu-Yuan Pan

*Address all correspondence to: pcchiang@ntu.edu.tw

Graduate Institute of Environmental Engineering, National Taiwan University, Taiwan

References

[1] Y.-W. Ko, P.-C. Chiang, C.L. Chuang, E.E. Chang, Kinetics of the Reaction Between Ozone and p-Hydroxybenzoic Acid in a Semi-batch Reactor, Ind. Eng. Chem. Res., 39 (2000) 635-641.

[2] P.-C. Chiang, Y.-W. Ko, Y.-M. Yang, Applying Mass Transfer Models for Controlling Organic Compounds in Ozonation Process, Environ Int, 23 (1997) 819-828.

[3] Y.M. Yang, Effects of ozone mass transfer on the formation and control of volatile organic compounds in drinking water, in: Graduate Institute of Environmental Engineering, National Taiwan University, Taipei, 1991.

[4] A. Ouedemi, J.C. Mora, R.S. Bes, Ozone absorption in water: Mass transfer and solubility, Ozone Sci. Eng., 9 (1987) 1-12.

[5] S. Sheffer, G.L. Esterson, Mass transfer and reaction kinetics in the ozone/tap water system, Water Res., 10 (1982) 383-389.

[6] I. Stankovic, Comparison of ozone and oxygen mass transfer in a laboratory and pilot plant operation, Ozone Sci. Eng., 10 (1988) 321-338.

[7] M.D. Gurol, Factors controlling the removal of organic pollutants in ozone reactors, J. Am. Water Wks. Assoc., 77 (1985) 55-60.

[8] P.V. Danckwerts, Gas Liquid Reactions, McGraw-Hill, New York, 1970.

[9] W.L. McCabe, J.C. Smith, P. Harriott, Unit operations of chemical engineering, 4 ed., McGraw-Hill, New York, 1985.

[10] W.J. DeCoursey, Absorption with chemical reaction: development of a new relation for the Danckwerts model, Chem. Eng. Sci., 29 (1974) 1867-1872.

[11] R. Turse, W. Rieman III, J. Phys. Chem., 65 (1961) 1821.

[12] J. Crank, The mathematics of Diffusion, Oxford Univ. Press, London, 1956.

[13] T.C. Huang, F.N. Tsai, The Canadian Journal of Chemical Engineering, 55 (1977) 302.

[14] H.T. Chang, B.E. Rittmann, Mathematical modeling of biofilm on activated carbon, Environ. Sci. Technol., 21 (1987) 273-280.

[15] C.H. Liang, P.C. Chiang, Mathematical model of the non-steady-state adsorption and biodegradation capacities of BAC filters, J Hazard Mater, 139 (2007) 316-322.

[16] C.H. Liang, P.C. Chiang, E.E. Chang, Modeling the behaviors of adsorption and biodegradation in biological activated carbon filters, Water research, 41 (2007) 3241-3250.

[17] A. Sakoda, J. Wang, M. Suzuki, Microbial activity in biological activated carbon bed by pulse responses., Water Sci. Technol., 34 (1996) 222-231.

[18] G.M. Walker, L.R. Weatherley, A simplified predictive model for biologically activated carbon fixed beds., Process. Biochem., 32 (1997) 327-335.

[19] R.J. Abumaizar, E.H. Smith, W. Kocher, Analytical model of dual-media biofilter for removal of organic air pollutants, J. Environ. Eng. ASCE, 123 (1997) 606-614.

[20] R.M. Hozalski, E.J. Bouwer, Non-steady state simulation of BOM removal in drinking water biofilters: model development., Water Res., 35 (2001) 198-210.

[21] B.N. Badriyha, V. Ravindran, W. Den, M. Pirbazari, Bioadsorber efficiency, design, and performance forecasting for alachlor removal, Water Res., 37 (2003) 4051-4072.

[22] B.E. Rittmann, P.L. McCarty, Substrate flux into biofilms of any thickness, J. Environ. Eng., ASCE, 107 (1981) 831-849.

[23] B.G. Oliver, J. Lawrence, Haloforms in Drinking Water: A Study of Precursors and Precursor Removal,, J. Amer. Water Works Assoc., 71 (1979) 161-163.

[24] O. Levenspiel, Chemical Reaction Engineering, third edition ed., John Wiley and Sons, 1999.

[25] P.-C. Chiang, E.E. Chang, Y.-W. Ko, J.-C. Lou, Balancing Disinfection Efficiency and THM Formation During Chlorination Theoretical Considerations, The Canadian Journal of Chemical Engineering, 75 (1997) 892-898.

[26] H. Collins, R. Selleck, Process Kinetics of Wastewater Chlorination, in, University of California, Berkeley, 1972.

[27] P.-C. Chiang, Y.-W. Ko, C.H. Liang, E.E. Chang, Modeling An Ozone Bubble Column for Predicting its Disinfection Efficiency and Control of Disinfection By-Products Formation, Chemosphere, 39 (1999) 55-70.

[28] J.G. Jacangelo, N.L. Patania, K.M. Reagau, E.M. Aieta, S.W. Krasner, M.J. McGuire, Ozonation: assessing its role in the formation and control of disinfection by-products, J. Amer. Water Works Assoc., 81 (1989).

[29] G.L. Amy, L. Tan, M.K. Davis, The effects of ozonation and activated carbon adsorption on trihalomethane speciation, War. Res., 25 (1991) 191-202.

[30] E.E. Chang, Y.-C. Wang, S.-Y. Pan, Y.-H. Chen, P.-C. Chiang, CO_2 Capture by Using Blended Hydraulic Slag Cement via a Slurry Reactor, Aerosol and Air Quality Research, 12 (2012) 1433-1443.

[31] S.N. Lekakh, C.H. Rawlins, D.G.C. Robertson, V.L. Richards, K.D. Peaslee, Kinetics of Aqueous Leaching and Carbonization of Steelmaking Slag, Metallurgical and Materials Transactions B, 39 (2008) 125-134.

[32] S.-Y. Pan, E.E. Chang, P.-C. Chiang, CO_2 Capture by Accelerated Carbonation of Alkaline Wastes: A Review on Its Principles and Applications, Aerosol and Air Quality Research, 12 (2012) 770-791.

[33] R.M. Santos, D. François, G. Mertens, J. Elsen, T. Van Gerven, Ultrasound-intensified mineral carbonation, Applied Thermal Engineering, 57 (2013) 154-163.

[34] S. Teir, S. Eloneva, C. Fogelholm, R. Zevenhoven, Fixation of carbon dioxide by producing hydromagnesite from serpentinite, Applied Energy, 86 (2009) 214-218.

[35] G. Costa, R. Baciocchi, A. Polettini, R. Pomi, C.D. Hills, P.J. Carey, Current status and perspectives of accelerated carbonation processes on municipal waste combustion residues, Environ Monit Assess, 135 (2007) 55-75.

[36] C. Lin, B. Chen, Characteristics of cross-flow rotating packed beds, Journal of Industrial and Engineering Chemistry, 14 (2008) 322-327.

[37] M. Wang, Controlling factors and mechanism of preparing needlelike CaCO3 under high-gravity environment, Powder Technology, 142 (2004) 166-174.

[38] T. Kelleher, J.R. Fair, Distillation studies in a high-gravity contactor, Ind Eng Chem Res, 35 (1996) 4646-4655.

[39] C. Tan, J. Chen, Absorption of carbon dioxide with piperazine and its mixtures in a rotating packed bed, Separation and Purification Technology, 49 (2006) 174-180.

[40] S.Y. Pan, P.C. Chiang, Y.H. Chen, C.S. Tan, E.E. Chang, Ex Situ CO_2 capture by carbonation of steelmaking slag coupled with metalworking wastewater in a rotating packed bed, Environ Sci Technol, 47 (2013) 3308-3315.

[41] E.E. Chang, C.H. Chen, Y.H. Chen, S.Y. Pan, P.C. Chiang, Performance evaluation for carbonation of steel-making slags in a slurry reactor, J Hazard Mater, 186 (2011) 558-564.

[42] H.Y. Sohn, J. Szekely, Reactions between solids through gaseous intermediates- I Reactions controlled by chemical kinetics, Chemical Engineering Science, 28 (1973) 1789-1801.

[43] H.Y. Sohn, The effects of reactant starvation and mass transfer in the rate measurement of fluid–solid reactions with small equilibrium constants, Chemical Engineering Science, 59 (2004) 4361-4368.

[44] P. Sandilya, D.P. Rao, A. Sharma, Gas-phase mass transfer in a centrifugal contactor, Ind Eng Chem Res, 40 (2001) 384-392.

[45] H.-H. Cheng, J.-F. Shen, C.-S. Tan, CO2 capture from hot stove gas in steel making process, International Journal of Greenhouse Gas Control, 4 (2010) 525-531.

[46] H. Liu, C. Kuo, Quantitative multiphase determination using the Rietveld method with high accuracy, Materials Letters, 26 (1996) 171-175.

[47] E.E. Chang, S.Y. Pan, Y.H. Chen, C.S. Tan, P.C. Chiang, Accelerated carbonation of steelmaking slags in a high-gravity rotating packed bed, J Hazard Mater, 227-228 (2012) 97-106.

[48] S.N. Lekakh, D.G.C. Robertson, C.H. Rawlins, V.L. Richards, K.D. Peaslee, Investigation of a Two-Stage Aqueous Reactor Design for Carbon Dioxide Sequestration Using Steelmaking Slag, Metallurgical and Materials Transactions B, 39 (2008) 484-492.

[49] S.-Y. Pan, E.G. Eleazar, E.-E. Chang, Y.-P. Lin, H. Kim, P.-C. Chiang, Systematic Approach to Determination of Optimum Gas-phase Mass Transfer Rate for High-gravity Carbonation Process of Steelmaking Slags in a Rotating Packed Bed, Applied energy, 148 (2015) 23-31.

[50] D.C. Arters, L.-S. Fan, Experimental methods and correlation of solid liquid mass transfer in fluidized beds, Chemical Engineering Science, 41 (1986) 107-115.

[51] S. Munjal, M.P. Dudukovic, P. Ramachandran, Mass-transfer in Rotating Packed Beds - I. Development of Gas-Liquid and Liquid-Solid Mass Transfer Correlations Chemical Engineering Science, 44 (1989) 2245-2256.

[52] H.H. Tung, R.S.H. Mah, Modeling liquid mass transfer in HIGEE separation process, Chemical Engineering Communication, 39 (1985) 147-153.

[53] K. Onda, H. Takeuchi, Y. Okumoto, Mass transfer coefficients between gas and liquid phases in packed columns, Journal of Chemical Engineering of Japan, 1 (1968) 56-62.

[54] R.H. Perry, C.H. Chilton, Chemical engineers' handbook, McGraw-Hill, New York, 1973.

IntechOpen

IntechOpen